Heterogeneous Catalysis

Deutsche Ausgabe: DOI: 10.1002/ange.201502206
Internationale Ausgabe: DOI: 10.1002/anie.201502206

Graphitic-Carbon Layers on Oxides: Toward Stable Heterogeneous Catalysts for Biomass Conversion Reactions**

*Haifeng Xiong, Thomas J. Schwartz, Nalin I. Andersen, James A. Dumesic, and Abhaya K. Datye**

Abstract: *Conversion of biomass-derived molecules involves catalytic reactions under harsh conditions in the liquid phase (e.g., temperatures of 250 °C and possibly under either acidic or basic conditions). Conventional oxide-supported catalysts undergo pore structure collapse and surface area reduction leading to deactivation under these conditions. Here we demonstrate an approach to deposit graphitic carbon to protect the oxide surface. The heterogeneous catalysts supported on the graphitic carbon/oxide composite exhibit excellent stability (even under acidic conditions) for biomass conversion reactions.*

Biomass-derived molecules are sustainable feedstocks for fuels, chemicals, and materials that need to be processed under varying aqueous phase conditions, including high temperatures and pressures as well as variable acidic, neutral, and basic media.[1] When used in a packed-bed reactor, the catalyst must be appropriately shaped to promote efficient mass transfer and minimize the pressure drop. While carbon is a suitable support for biorenewable conversions, it is difficult to prepare pelletized carbon materials with high mechanical stability.[2] On the other hand, oxide supports are available in a variety of sizes and shapes and possess excellent mechanical stability, making them suitable for large-scale industrial applications. However, oxide supports undergo structural collapse and phase transformation,[3] leading to deactivation in liquid phase reactions for biomass conversion, even at a pH of 7.[4]

One recent approach used for improving hydrothermal stability is to deposit pyrolyzed sugars on the oxide.[5] The stability of these materials has been investigated under static conditions in an autoclave. We have found that these materials may not be suitable for use under harsh aqueous-phase conditions in a continuous fixed-bed reactor, because the carbon may be leached from the material leading to catalyst deactivation (see the Supporting Information (SI), Figures S1 and S2). The oxygen-containing carbonaceous species derived from sugars or other biomass-derived compounds may be reactive and undergo reactions in the presence of liquid water and the metal catalyst at elevated temperatures. We have also found that the pyrolyzed sugars may not survive under strongly acidic or basic conditions, both of which are important for biomass conversions. A more stable form of carbon is needed for the harsh conditions necessitated by reactions in biomass conversion.[6]

Here, we report the synthesis of graphitic carbon on oxides by chemical vapor deposition (CVD). This approach is applicable for the preparation of graphitic carbon on pelletized oxide supports. Because γ-Al_2O_3 is a versatile and widely used support, possessing high surface area and mechanical stability in pelletized form, we have used it as an example to demonstrate the applicability of our approach. The graphitic carbon/alumina composite (gc-Al_2O_3) was prepared by CVD at 900 °C using CH_4 as the reactant (Scheme 1). The decomposition time of CH_4 varied from 0.5–6 h, and the relative carbon loadings for the gc-Al_2O_3 ranged from 6.4-45.2 wt % (Table S1). When the decomposition time of CH_4 is >6 h, the surface area of the obtained gc-Al_2O_3 composite is significantly decreased, indicating pore blockage by carbon.

The graphitic carbon layer is more stable than carbon deposited from the pyrolysis of sugars. In flowing air, the

[*] Dr. H. F. Xiong, N. I. Andersen, Prof. A. K. Datye
Department of Chemical and Biological Engineering
University of New Mexico, MSC 01 1120
Albuquerque, NM 87131 (USA)
E-mail: datye@unm.edu
T. J. Schwartz, Prof. J. A. Dumesic
Department of Chemical and Biological Engineering
University of Wisconsin-Madison
Madison, WI 53706 (USA)

[**] This work is supported by the Center for Biorenewable Chemicals (CBiRC) supported by NSF under grant No. EEC-0813570. We thank Dr. A. S. Ali for ICP-AES measurements and Dr. Hien Pham for HRTEM. T.J.S. acknowledges support from the NSF Graduate Research Fellowship Program under grant No. DGE-1256259. Any opinions, findings, and conclusions or recommendations expressed in this material are those of the authors and do not necessarily reflect the views of the National Science Foundation.

Supporting information for this article is available on the WWW under http://dx.doi.org/10.1002/anie.201502206.

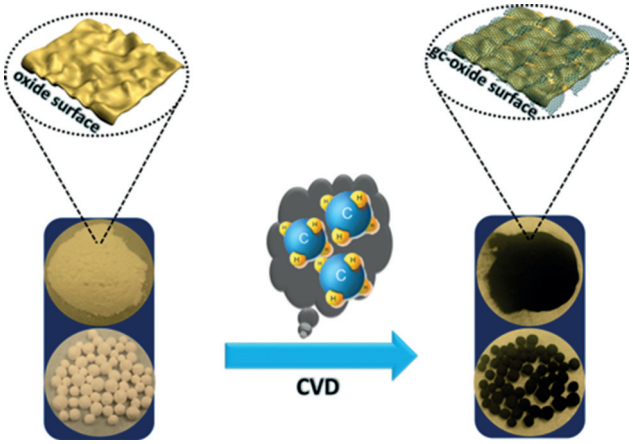

Scheme 1. Preparation of graphitic carbon/oxide composites that is applicable to powders as well as pellets.

carbon on the gc-Al_2O_3 becomes oxidized at ca. 500 °C compared to 250 °C for pyrolytic carbon (SI). Figure S3 shows the TGA profiles of the γ-Al_2O_3 and gc-Al_2O_3 composites in a flow of air. Table S2 presents a summary of the temperature at which the gc-Al_2O_3 is lost. The oxidation temperature of the gc-Al_2O_3 shifted to a higher temperature as the carbon content was increased, indicating that the gc-Al_2O_3 with a high carbon loading was more difficult to oxidize.

The hydrothermal stability of the alumina, with and without the graphitic carbon coating, was assessed in an autoclave using water under static conditions at 220 °C and autogenic pressure for 12 h. The phase compositions of the γ-Al_2O_3 and gc-Al_2O_3 before hydrothermal treatment are shown in Figure 1 a. As seen in this Figure, the increase of

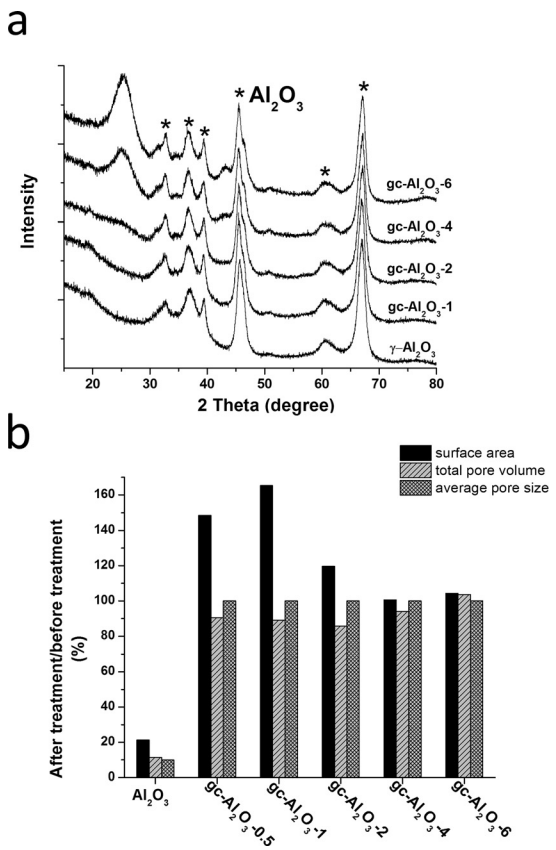

Figure 1. XRD patterns of a) gc-Al_2O_3 with different deposition time of CH_4; b) the ratios after hydrothermal treatment to before hydrothermal treatment (expressed as %) of surface area, total pore volume, and average particle sizes for γ-Al_2O_3 and gc-Al_2O_3.

the CH_4 deposition time leads to the growth of a diffraction peak centered at 24°, whereas the other diffraction peaks corresponding to γ-Al_2O_3 do not change. The diffraction peak at 24° corresponds to graphitic carbon. After the γ-Al_2O_3 was treated in liquid water at 220 °C for 12 h, the XRD pattern of γ-Al_2O_3 shows well-defined diffraction peaks of the boehmite phase (Figure S5), indicating that the alumina has reacted with water. For the gc-Al_2O_3 composites, the XRD patterns of the gc-Al_2O_3 with low carbon loadings showed weak diffraction peaks of boehmite after treatment, whereas no significant change was found in the XRD pattern of gc-Al_2O_3 with high carbon loadings after treatment (Figure S5). These results indicate that the deposition of graphitic carbon onto γ-Al_2O_3 can effectively improve the stability of γ-Al_2O_3 in liquid water at elevated temperatures. The N_2 physisorption data of the γ-Al_2O_3 and gc-Al_2O_3 before and after the treatment are shown in Table S1 and Figure 1. The total pore volume decreased as the carbon loading was increased, resulting in surface areas ranging from 77–130 $m^2 g^{-1}$. When the uncoated γ-Al_2O_3 was treated in static water at 220 °C for 12 h, the surface area decreased by 80 % and the total pore volume decreased by 90 % (Figure 1). The gc-Al_2O_3 (gc-Al_2O_3-4 and gc-Al_2O_3-6) showed no significant decrease in surface area, pore volume and average pore size after treatment as compared to the catalyst before treatment. The surface areas of gc-Al_2O_3 with low carbon loadings increased dramatically after hydrothermal treatment. This behavior is attributed to a partial structural change of the gc-Al_2O_3, revealed by the XRD results. These results show that the gc-Al_2O_3 materials with high carbon loadings have superior hydrothermal stability compared to γ-Al_2O_3 in static liquid water at elevated temperatures.

The SEM images of γ-Al_2O_3 and gc-Al_2O_3 with the highest carbon loading (gc-Al_2O_3-6) are shown in Figures 2 and S6. The SEM image of γ-Al_2O_3 shows a spherical morphology (Figure 2) which is preserved after carbon deposition in the gc-Al_2O_3 (gc-Al_2O_3-6).

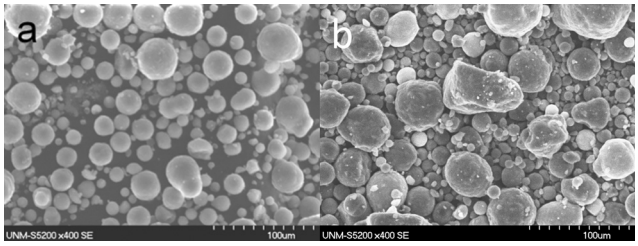

Figure 2. SEM images of a) γ-Al_2O_3; b) gc-Al_2O_3-6.

We acquired elemental carbon maps by energy-filtered transmission electron microscopy (EFTEM) to investigate the nanoscale distribution of carbon species on the gc-Al_2O_3-6 sample. Figure 3 shows the bright field TEM image (a), the carbon K-edge EFTEM image (b), and the oxygen K-edge EFTEM image (c). The bright-red regions in Figure 3 b indicate that carbon is deposited uniformly on the oxide support. Images of other carbon containing samples are

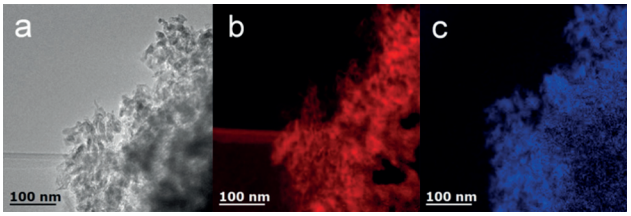

Figure 3. TEM and energy-filtered TEM (EFTEM) images of gc-Al_2O_3-6: a) TEM image; b) elemental carbon map; c) elemental oxygen map.

shown in Figure S7. In Figure 3b, the underlying holey carbon film shows a lower intensity than the graphitic carbon, whereas images of samples with lower loading (Figure S7) show the carbon film having higher contrast.

Raman spectroscopy was used to determine the type of carbon, degree of structural ordering, and the presence of defects in the carbon materials.[7] An optical micrograph of gc-Al_2O_3 (gc-Al_2O_3-6, Figure 4a) shows similar spherical morphology to that observed by SEM (Figure 2). A Raman spectroscopy mapping corresponding to the square in Figure 4a is shown in Figure 4b. Graphitic carbon formed on the γ-Al_2O_3 is indicated in yellow. The centers of some particles appear to show lower intensity in Figure 4b, but the higher magnification view in Figure 4d confirms the presence of carbon uniformly throughout the alumina spheres. The Raman spectrum obtained from the gc-Al_2O_3 (Figure 4c, curve 1) shows two peaks located at 1350 and 1590 cm^{-1}, whereas pyrolyzed carbon on alumina or blank alumina show no such features (Figure 4c, curves 2 and 3). The first peak at ca. 1350 cm^{-1} corresponds to the disorder-induced band (D-band), the second peak at about 1590 cm^{-1} corresponds to the tangential band (G-band).[8] The peaks were deconvoluted and the I_G/I_D ratio of gc-Al_2O_3-6 is 0.71, indicating that the carbon overlayer is highly graphitized.[9] Both the overview and cross section maps show that graphitic carbon is dispersed on the surface of γ-Al_2O_3 (Figures 4b and S8). A high magnification 3D image of the sample is shown in Figure 4d. This Figure is a composite of the 2D images acquired from the surface of the particle, and then focusing progressively on sections below the surface (in increments of 10 nm). The image shows domains of 0.1–0.4 μm, which correspond to graphitic carbon uniformly dispersed on the alumina surface (Figure 4d).

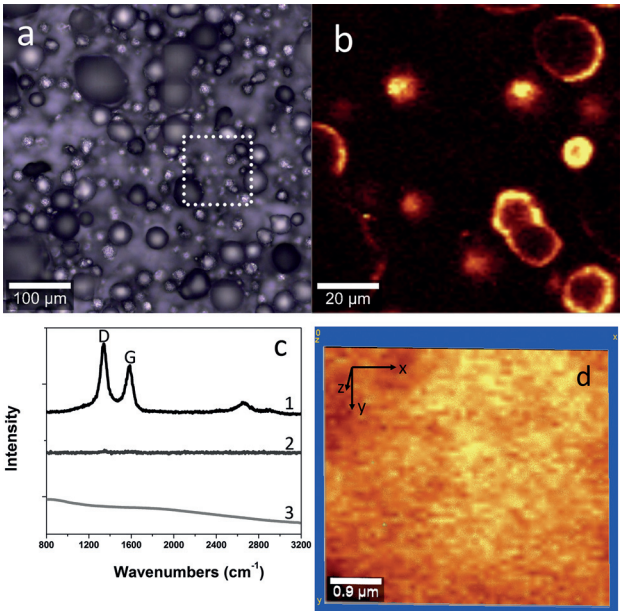

Figure 4. Raman spectroscopy mapping and spectra of gc-Al_2O_3-6 prepared by chemical vapor deposition: a) Optical micrograph of the gc-alumina sample; b) Raman spectroscopy map of the region marked in the box in (a); c) Raman spectrum of the gc-alumina (1), uncoated alumina (2), and 10% carbon on alumina deposited via pyrolysis of sugars (3); d) high-magnification view showing a composite of 10 nm sections of a spherical particle showing uniform distribution of carbon.

High-resolution transmission electron microscopy (HRTEM) was used to investigate the morphology and distribution of the graphitic carbon species on the γ-Al_2O_3. The representative HRTEM images are shown in Figures 5 and S9. We found that the presence of lattice fringes with d-spacing of 1.8 and 2.5 Å correspond to γ-Al_2O_3, whereas the 3.4 Å lattice fringe corresponds to the (002) planes of graphitic carbon.[10] The graphitic carbon can be seen to cover the alumina surface. Furthermore, the number of the graphitic carbon layers on the gc-Al_2O_3-6 was calculated and it is in agreement with the TEM observation (SI).

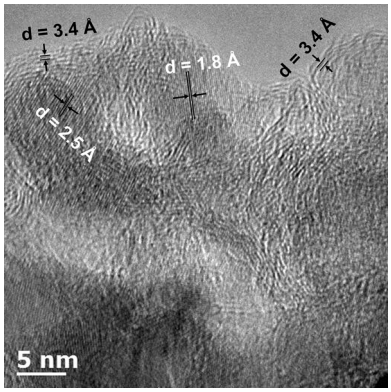

Figure 5. High-resolution TEM image of gc-Al_2O_3.

Two biomass-related reactions were used as model reactions to demonstrate the stability of heterogeneous catalysts under harsh, aqueous-phase conditions when using the graphitic carbon/Al_2O_3 composite as a support. The stability of the gc-Al_2O_3 supported Pt catalyst (1 wt% Pt loading) was investigated in neutral conditions for aqueous-phase reforming (APR) of ethylene glycol (EG) at 250 °C and 70 bar. The catalytic activity as a function of time on stream for Pt/γ-Al_2O_3 and Pt/gc-Al_2O_3 catalysts is shown in Figure 6. As can be seen, the Pt/gc-Al_2O_3 catalyst showed a two-fold higher activity than Pt/γ-Al_2O_3 for APR of EG. ICP-OES results showed that Pt and Al were detected in the liquid phase product, indicating that catalyst leaching was occurring for the Pt/γ-Al_2O_3 catalyst during the first 250 h of the run. No Pt or Al was found with the Pt/gc-Al_2O_3 catalyst. The XRD results of the spent Pt/γ-Al_2O_3 catalyst showed that the γ-Al_2O_3 phase was completely converted to boehmite, whereas the gc-Al_2O_3 did not change under APR reaction conditions (Figure S10). The STEM images of the Pt catalysts before and after reaction showed that the Pt particles on the Pt/γ-Al_2O_3 catalyst increased in size after reaction (Figures 6d and S11), while the Pt particles did not change significantly for the Pt/gc-Al_2O_3 catalyst. Thus, the deactivation of the Pt/γ-Al_2O_3 catalyst can be attributed to Pt sintering and catalyst leaching, which is caused by the alumina reacting with liquid water, whereas the Pt/gc-Al_2O_3 catalyst was stable and maintained

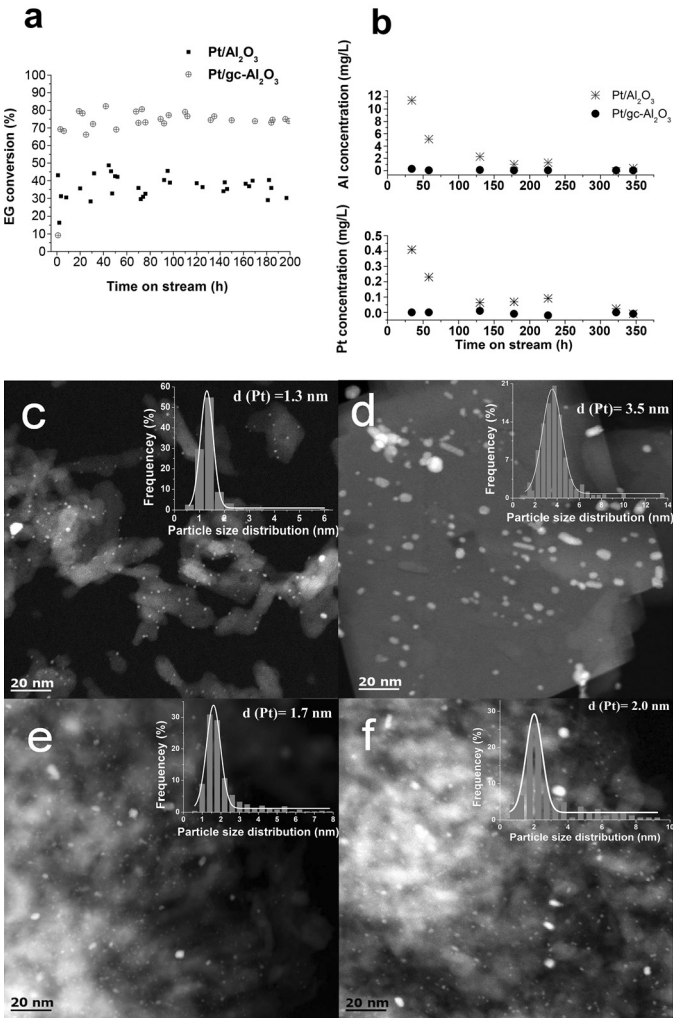

Figure 6. a) Catalyst activity as a function of time on stream for Pt catalysts for aqueous-phase reforming of ethylene glycol (EG) at 250 °C and 70 bar; b) elemental Pt and Al concentrations in the solutions collected during aqueous-phase reforming of ethylene glycol (2 wt% EG/H_2O); c) STEM image of fresh Pt/γ-Al_2O_3; d) STEM image of spent Pt/γ-Al_2O_3 after APR reaction; e) STEM image of fresh Pt/gc-Al_2O_3; f) STEM image of spent Pt/gc-Al_2O_3 after APR reaction.

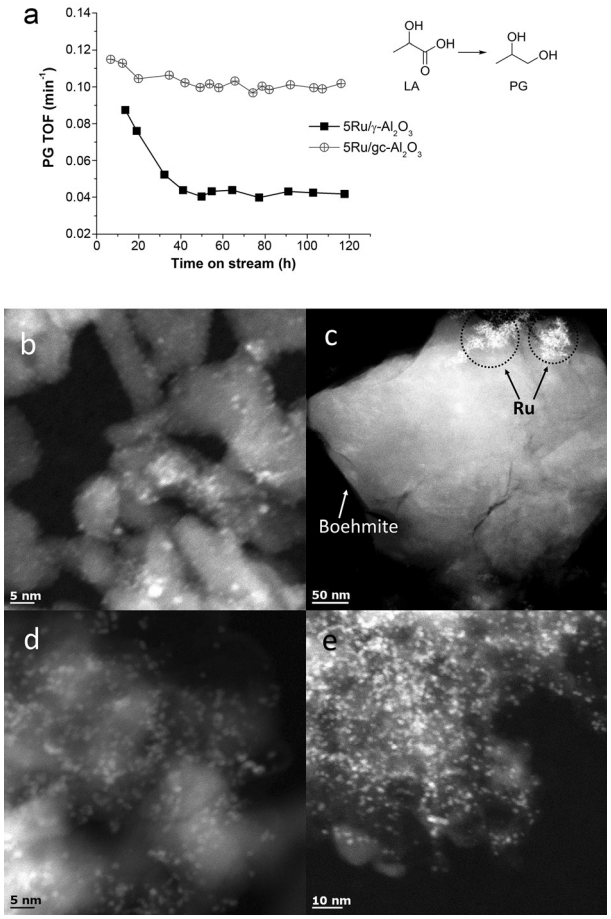

Figure 7. a) Specific propylene glycol formation rate as a function of time on stream for two Ru catalysts (5 wt% Ru) in liquid phase hydrogenation of lactic acid (LA) to propylene glycol (PG) at 120 °C and 500 psi (5 wt% LA/H_2O); b) STEM image of fresh Ru/γ-Al_2O_3; c) STEM image of spent Ru/γ-Al_2O_3 after liquid phase hydrogenation; d) STEM image of fresh Ru/gc-Al_2O_3; e) STEM image of spent Ru/gc-Al_2O_3 after liquid phase hydrogenation.

high activity at the high pressure and temperature encountered during APR.

The hydrothermal stability of the gc-Al_2O_3-supported Ru catalyst (5 wt% Ru loading) was also investigated under acidic conditions during lactic acid hydrogenation in the aqueous phase (Figure 7). The Ru/gc-Al_2O_3 was stable during the run, whereas the Ru/γ-Al_2O_3 catalyst exhibited deactivation during the first 40 h of reaction, after which the catalyst appeared to be stable. Similar catalytic behavior was also observed on Ru/γ-Al_2O_3 and Ru/gc-Al_2O_3 with 1 wt% Ru loading (Figure S12). STEM images for the spent catalyst showed that for the Ru/γ-Al_2O_3 catalyst, not only did the γ-Al_2O_3 transform into boehmite, but the Ru particles also increased in size (circles in Figure 7c). However, the Ru particles on the Ru/gc-Al_2O_3 catalyst maintained their high dispersion with Ru particle size of 1–3 nm. Thus, the gc-Al_2O_3 supported Ru catalyst exhibits superior hydrothermal stability under acidic, aqueous-phase conditions.

In summary, we have developed a method to deposit graphitic carbon layers on oxide surfaces by chemical vapor deposition that allows these materials to be used as heterogeneous catalysts that are able to withstand severe hydrothermal conditions in liquid water under both neutral and acidic conditions. While the improved hydrothermal stability of amorphous, pyrolytic carbon-coated alumina has been demonstrated previously, such amorphous carbon is reactive and susceptible to hydrolytic attack in the presence of the active catalyst phase. In contrast, graphitic carbon is less reactive and is better able to withstand the harsh conditions that are encountered during the conversion of biorenewables. The deposition of graphitic carbon through vapor phase routes allows deposition within preformed structures as shown in Scheme 1, in which pellets of alumina were coated with carbon. The CVD approach presented here allows modification of the vast library of preformed oxide-based

supports with appropriate pore structure and external shapes that are already commercially available. By depositing graphitic carbon, we can tailor these supports for biomass conversion and upgrading, especially for use in packed-bed reactors, for which suitable pore structure and mechanical strength is desired.

Keywords: biomass · graphitic carbon · heterogeneous catalysis · hydrogenation · stability

How to cite: *Angew. Chem. Int. Ed.* **2015**, *54*, 7939 – 7943
Angew. Chem. **2015**, *127*, 8050 – 8054

[1] a) R. D. Cortright, R. R. Davda, J. A. Dumesic, *Nature* **2002**, *418*, 964 – 967; b) S. Crossley, J. Faria, M. Shen, D. E. Resasco, *Science* **2010**, *327*, 68 – 72.
[2] D. S. Su, S. Perathoner, G. Centi, *Chem. Rev.* **2013**, *113*, 5782 – 5816.
[3] P. A. Zapata, J. Faria, M. P. Ruiz, R. E. Jentoft, D. E. Resasco, *J. Am. Chem. Soc.* **2012**, *134*, 8570 – 8578.
[4] a) H. Xiong, H. N. Pham, A. K. Datye, *Green Chem.* **2014**, *16*, 4627 – 4643; b) K. Koichumanova, A. K. K. Vikla, D. J. M. de Vlieger, K. Seshan, B. L. Mojet, L. Lefferts, *ChemSusChem* **2013**, *6*, 1717 – 1723; c) D. J. M. de Vlieger, B. L. Mojet, L. Lefferts, K. Seshan, *J. Catal.* **2012**, *292*, 239 – 245; d) R. M. Ravenelle, J. R. Copeland, A. H. Pelt, J. C. Crittenden, C. Sievers, *Top. Catal.* **2012**, *55*, 162 – 174.
[5] a) H. Xiong, H. N. Pham, A. K. Datye, *J. Catal.* **2013**, *302*, 93 – 100; b) H. N. Pham, A. E. Anderson, R. L. Johnson, K. Schmidt-Rohr, A. K. Datye, *Angew. Chem. Int. Ed.* **2012**, *51*, 13163 – 13167; *Angew. Chem.* **2012**, *124*, 13340 – 13344; c) A. L. Jongerius, J. R. Copeland, G. S. Foo, J. P. Hofmann, P. C. A. Bruijnincx, C. Sievers, B. M. Weckhuysen, *ACS Catal.* **2013**, *3*, 464 – 473.
[6] a) J. Matthiesen, T. Hoff, C. Liu, C. Pueschel, R. Rao, J.-P. Tessonnier, *Chin. J. Catal.* **2014**, *35*, 842 – 855; b) E. Lam, J. H. T. Luong, *ACS Catal.* **2014**, *4*, 3393 – 3410.
[7] a) A. Sadezky, H. Muckenhuber, H. Grothe, R. Niessner, U. Pöschl, *Carbon* **2005**, *43*, 1731 – 1742; b) M. Knauer, M. E. Schuster, D. Su, R. Schlögl, R. Niessner, N. P. Ivleva, *J. Phys. Chem. A* **2009**, *113*, 13871 – 13880.
[8] a) H. Xiong, M. Moyo, M. A. Motchelaho, Z. N. Tetana, S. M. A. Dube, L. L. Jewell, N. J. Coville, *J. Catal.* **2014**, *311*, 80 – 87; b) Z. Wu, W. Li, Y. Xia, P. Webley, D. Zhao, *J. Mater. Chem.* **2012**, *22*, 8835 – 8845.
[9] H. Xiong, M. Moyo, M. A. M. Motchelaho, L. L. Jewell, N. J. Coville, *Appl. Catal. A* **2010**, *388*, 168 – 178.
[10] M. H. Rümmeli, C. Kramberger, A. Grüneis, P. Ayala, T. Gemming, B. Büchner, T. Pichler, *Chem. Mater.* **2007**, *19*, 4105 – 4107.

Received: March 9, 2015
Published online: May 14, 2015

